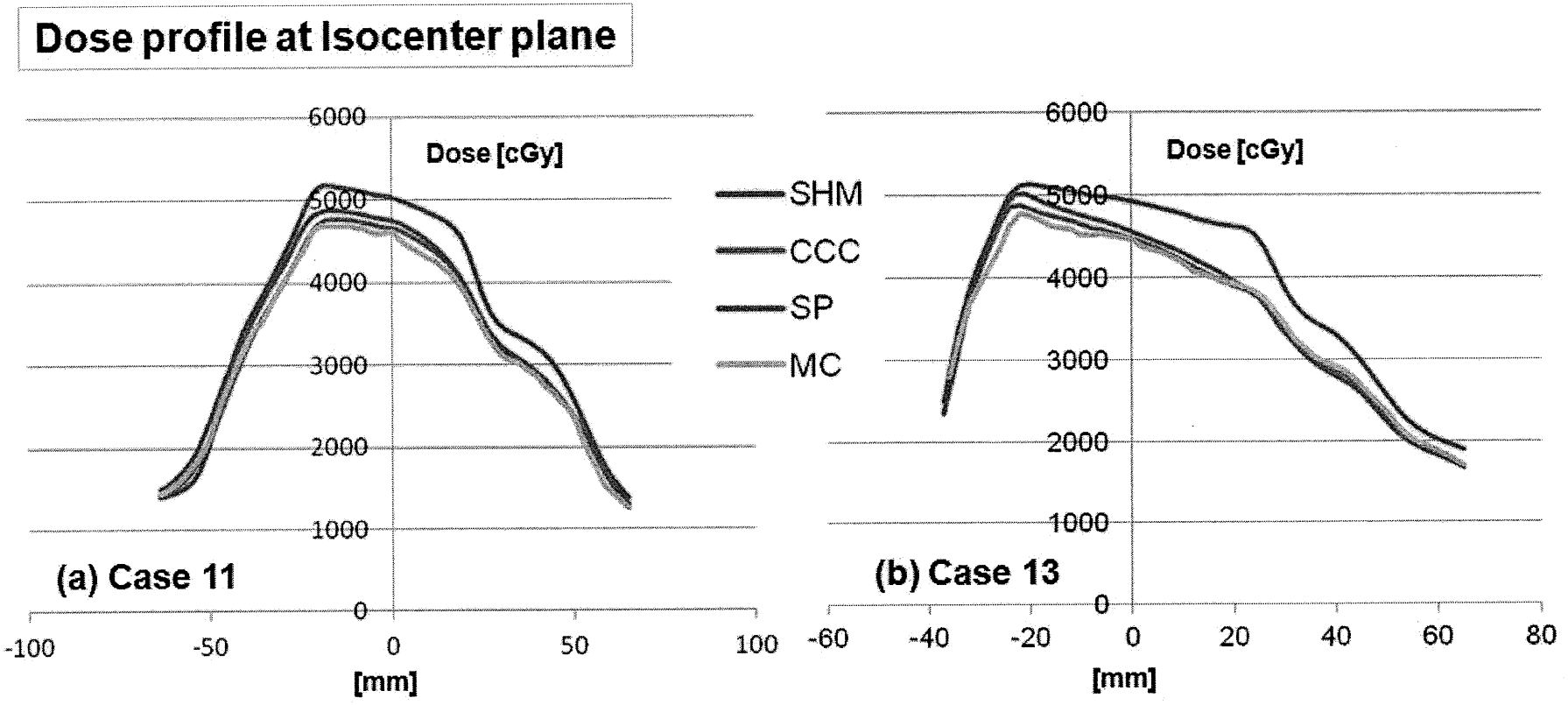
Dose profile at Isocenter plane
Dose [cGy]
6000
5000
4000
3000
2000
1000
0
-100
-50
0
50
100
[mm]
(a) Case 11
SHM
CCC
SP
MC
Dose [cGy]
6000
5000
4000
3000
2000
1000
0
-60
-40
-20
0
20
40
60
80
[mm]
(b) Case 13

Figure 4

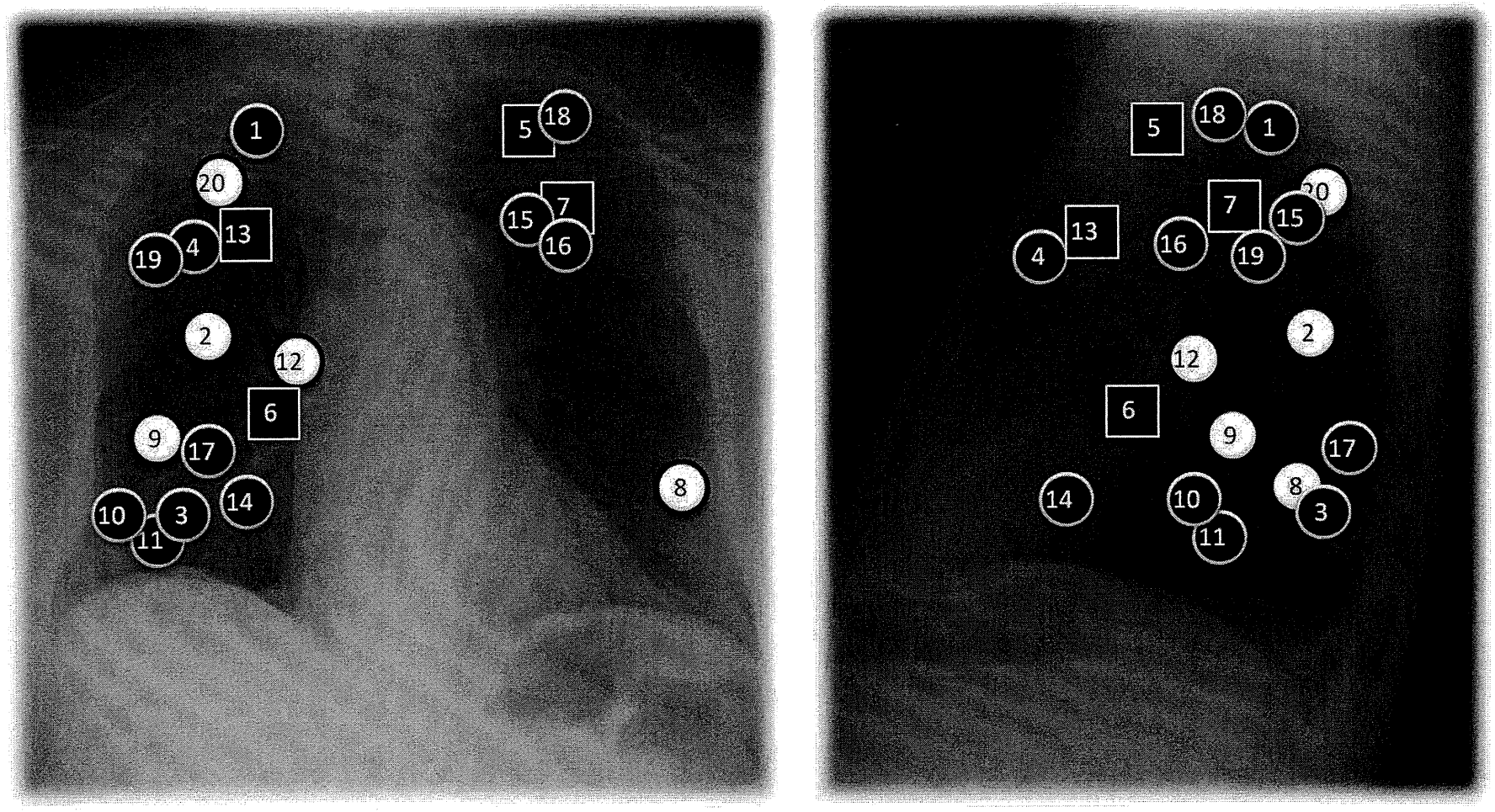
1
20
13
19
4
2
12
6
9
17
10
3
14
11
5
18
7
15
16
8
5
18
1
20
7
15
13
4
16
19
2
12
6
9
17
14
10
8
3
11

Figure 5

Original Article

Extended Field Stereotactic Radiosurgery for Recurrent Glioblastoma

Tomoyuki Koga, MD[1]; Keisuke Maruyama, MD, PhD[1]; Minoru Tanaka, MD, PhD[1]; Yasushi Ino, MD, PhD[1,2]; Nobuhito Saito, MD, PhD[1]; Keiichi Nakagawa, MD, PhD[3]; Junji Shibahara, MD, PhD[4]; and Tomoki Todo, MD, PhD[1,2]

BACKGROUND: Stereotactic radiosurgery (SRS) is among the few therapeutic options for glioblastoma that recurs after standard radiation and chemotherapy, but its efficacy has been limited. **METHODS:** Since November 2007, the authors have modified the clinical target volume by adding a 0.5- to 1-cm margin to the gadolinium-enhanced area (extended field SRS), in contrast to conventional SRS using no margin to set the clinical target volume. A total of 35 recurred glioblastoma lesions in 9 patients were treated with conventional SRS between December 1990 and January 2007, and 14 lesions in 9 patients were treated with extended field SRS. **RESULTS:** The median follow-up periods were 7 months (range, 3-29 months) and 8 months (range, 6-27 months), respectively. The local control rate was 47% for conventional SRS and 93% for extended field SRS ($P = .0035$), and the numbers of radiation necrosis observed in SRS-treated lesions were 2 and 4, respectively. The median overall survival from the diagnosis was 24 months (range, 14-57 months) for conventional SRS and 21 months (range, 15-51 months) for extended field SRS (statistically not significant). Seven patients treated with conventional SRS died during follow-up, 6 from progression of the SRS-treated tumor, whereas 7 patients treated with extended field SRS died during follow-up, 6 from remote intracerebral dissemination. **CONCLUSIONS:** Extended field SRS was superior to conventional SRS in the local control of small recurrent lesions of glioblastoma, although a further device to suppress remote dissemination may be necessary to increase survival. ***Cancer* 2011;000:000–000.** © *2011 American Cancer Society.*

KEYWORDS: glioblastoma, glioma, gamma knife, stereotactic radiosurgery, radiation therapy, recurrence.

INTRODUCTION

Glioblastoma is a highly malignant and aggressive tumor of the central nervous system that corresponds to grade IV of the World Health Organization histological classification.[1] The current standard treatment for glioblastoma is a maximal resection with functional preservation, followed by radiation and chemotherapy. When temozolomide is used for chemotherapy, the median survival is 14.6 months after initial presentation,[2] and ranges from 5 to 13 months after recurrence.[3,4] Because of the aggressive and invasive nature of the tumor, recurrence is seen in >90% of patients.[5] The most common pattern of recurrence is local regrowth[6]; therefore, successful local control should lead to prolongation of patients' survival. Various local treatment strategies have been attempted, including repeated operations, conformal radiotherapy, brachytherapy, and local chemotherapy.[7]

Although stereotactic radiosurgery (SRS) is an option as salvage treatment for recurrent glioblastoma in clinical settings, the role of SRS is still limited for glioma. SRS is useful in controlling relatively well-demarcated glioma such as ependymoma, pilocytic astrocytoma, and pleomorphic xanthoastrocytoma.[8-13] However, the majority of glioma is infiltrative to brain parenchyma and is difficult to target with SRS. A randomized controlled study proved that there was no benefit in upfront SRS before conventional fractionated radiation therapy for patients with glioblastoma.[14] Several reports indicate the usefulness of adjuvant SRS at recurrence for glioblastoma, median survival time after SRS being 4.6 to 16 months,[15-20] although a randomized study is needed to prove efficacy. The major cause of treatment failure in managing recurrent glioblastoma by SRS is assumed to be that the highly conformal irradiation spares the surrounding tissue, which is presumably infiltrated with viable tumor cells.[21-23] With the intent to cover such tissue surrounding the bulk of tumor as much as possible, we changed the treatment protocol of SRS for recurrent glioblastoma lesions by extending the clinical target volume.[24] We present the early results of this newly applied treatment strategy.

Corresponding author: Tomoki Todo, MD, PhD, Division of Innovative Cancer Therapy, Institute of Medical Science, University of Tokyo, 4-6-1 Shirokanedai, Minato-ku, Tokyo 108-8639 Japan; Fax: (011) + 81-3-6409-2147; toudou-nsu@umin.ac.jp

[1]Department of Neurosurgery, University of Tokyo Hospital, Tokyo, Japan; [2]Translational Research Center, University of Tokyo Hospital, Tokyo, Japan; [3]Department of Radiology, University of Tokyo Hospital, Tokyo, Japan; [4]Department of Pathology, University of Tokyo Hospital, Tokyo, Japan

DOI: 10.1002/cncr.27372, **Received:** June 12, 2011; **Revised:** September 19, 2011; **Accepted:** October 24, 2011, **Published online** in Wiley Online Library (wileyonlinelibrary.com)

Table 1. Characteristics of the Patients Who Received Conventional SRS

Case No.	Age, y/Sex	Initial Hx	Initial Tx	Time from Dx to 1st SRS, mo	No. of Lesions	Controlled Lesions	Time to Local Relapse, mo	Last F/U, mo after 1st SRS	Outcome
1	25/M	Glioblastoma	EBRT, ACNU	22	3	1/3	4	4	Lost to F/U
2	40/M	Glioblastoma	EBRT, ACNU	17	1	0/1	9	29	Dead
3	43/M	Glioblastoma	EBRT, ACNU	10	3	0/3	10	16	Dead
4	62/M	AA	EBRT, ACNU	1	1	NA	NA	13	Dead
5	43/M	Glioblastoma	EBRT, ACNU	6	5	3/5	7	8	Lost to F/U
6	59/F	Glioblastoma	EBRT, CE	15	6	1/6	6	7	Dead
7	17/F	Glioblastoma	BNCT, TMZ	14	6	5/6	6	6	Dead
8	64/F	Glioblastoma	EBRT, ACNU	19	1	0/1	1	3	Dead
9	54/M	Glioblastoma	EBRT, TMZ	51	9	6/9	5	6	Dead

Abbreviations: AA, anaplastic astrocytoma; ACNU, nimustine hydrochloride; BNCT, boron neutron capture therapy; CE, carboplatin and etoposide; Dx, diagnosis of glioblastoma; EBRT, external beam radiotherapy; F, female; F/U, follow-up; Hx, histology; M, male; NA, data not available; SRS, stereotactic radiosurgery; TMZ, temozolomide; Tx, treatment.

Table 2. Characteristics of the Patients Who Received Extended Field SRS

Case No.	Age/Sex	Primary Hx	Primary Tx	Time from Dx to 1st SRS, mo	No. of Lesions	Controlled Lesions	Time to Local Relapse, mo	Last F/U, mo after 1st SRS	Outcome
1	53/M	Glioblastoma	EBRT, TMZ	17	1	1/1	—	27	Dead
2	27/M	Glioblastoma	EBRT, TMZ	39	1	0/1	1	12	Dead
3	43/M	AA	EBRT, TMZ	18	1	1/1	—	8	Dead
4	63/M	Glioblastoma	EBRT, TMZ	13	1	1/1	—	10	Dead
5	36/M	DA	EBRT, TMZ	9	3	3/3	—	8	Dead
6	66/F	Glioblastoma	EBRT, TMZ	9	3	3/3	—	6	Dead
7	47/M	Glioblastoma	EBRT, TMZ	12	2	2/2	—	7	Dead
8	58/F	Glioblastoma	EBRT, TMZ	6	1	1/1	—	12	Alive
9	79/F	Glioblastoma	EBRT, TMZ	9	1	1/1	—	8	Alive

Abbreviations: AA, anaplastic astrocytoma; DA, diffuse astrocytoma; Dx, diagnosis of glioblastoma; EBRT, external beam radiotherapy; F, female; F/U, follow-up; Hx, histology; M, male; SRS, stereotactic radiosurgery; TMZ, temozolomide; Tx, treatment.

MATERIALS AND METHODS

Patient Population

Nine patients with recurrent glioblastoma underwent 14 sessions of conventional SRS for 35 lesions using the Leksell Gamma Knife at our institute between December 1990 and January 2007 (Table 1). The median patient age was 43 years (range, 17-64 years). The median Karnofsky Performance Scale score at the first presentation was 90% (range, 80%-90%), and the median Karnofsky Performance Scale score at the time of first SRS for recurrence was 90% (range, 40%-90%). All the patients underwent surgical resection followed by radiation and chemotherapy at the primary onset. Primary lesions were histologically diagnosed as glioblastoma in 8 patients. In 1 patient, the primary lesion was diagnosed as anaplastic astrocytoma, but the recurred lesion was histologically confirmed as glioblastoma after resection. As primary treatment, external beam radiotherapy was applied for 8 patients with the median total dose of 60 grays (Gy; range, 48-80 Gy). Twenty-five of the 35 treated lesions (71%) were within the clinical target volume of the preceding radiotherapy. One patient underwent boron neutron capture therapy. For adjuvant chemotherapy, nimustine hydrochloride was used for 7 patients, carboplatin and etoposide for 1 patient, and temozolomide for 1 patient. The median interval between the time of diagnosis as glioblastoma and the recurrence was 14.5 months (range, 1-51 months).

Nine patients with recurrent glioblastoma underwent 11 sessions of extended field SRS for 14 lesions from November 2007 to April 2010 (Table 2). The extended field SRS was applied to a single recurrent lesion or 2 separate lesions that were $\leq$20 mm in diameter. The median age of this patient group was 53 years (range, 27-79 years). The median Karnofsky Performance Scale score at the first presentation was 90% (range, 80%-90%), and the median Karnofsky Performance Scale score at the time of first SRS for recurrence was 70% (range, 40%-90%).

Seven of these 9 patients underwent surgical resection, and 2 patients received stereotactic biopsy. The initial histological diagnosis was glioblastoma in 7 patients, anaplastic astrocytoma in 1 patient, and diffuse astrocytoma in 1 patient. In the latter 2 patients, lesions were histologically confirmed as glioblastoma at the time of recurrence. All of the 9 patients underwent external beam radiation therapy, with the median total dose of 70 Gy (range, 60-80 Gy). Ten of 14 treated lesions (71%) were within the clinical target volume of the preceding radiotherapy. Seven of them were treated with concomitant and adjuvant temozolomide therapy until the time of SRS for recurrences. For 1 patient, temozolomide was discontinued at the third cycle and nimustine hydrochloride administration was started, because of eruption and thrombocytopenia caused by temozolomide. The other patient received nimustine hydrochloride during radiation, and adjuvant temozolomide therapy was applied for up to 21 cycles until he denied the continuation of the chemotherapy. The median interval between the time of diagnosis as glioblastoma and the recurrence was 12 months (range, 6-39 months).

Conventional SRS

After their heads had been immobilized in the Leksell stereotactic head frame, the patients underwent stereotactic magnetic resonance imaging (MRI) to obtain precise information on the shape, volume, and 3-dimensional coordinates of the tumors. Image-integrated treatment planning was performed jointly by neurosurgeons and radiation oncologists with commercially available software (Leksell GammaPlan; Elekta Instruments AB, Stockholm, Sweden). The clinical target volume was defined as the gadolinium-enhanced lesion without any margin. In principle, the desired dose applied to the margin of each gadolinium-enhanced lesion was 20 Gy. The prescription dose was occasionally reduced because of the tumor volume, the location of lesions, and/or the clinical status of the patient. The median clinical target volume of conventional SRS was 15 cm^3 (range, 3-47 cm^3).

Extended Field SRS

The methods of head fixation, obtaining stereotactic images, and treatment planning and the principle for dose prescription were the same as conventional SRS. The difference was the definition of the clinical target volume, which was extended by adding a 0.5- to 1-cm margin to the periphery of the gadolinium-enhanced lesion. Margin was extended up to a maximum of 1 cm in all directions. By using a dose-volume histogram, the volume that received >20 Gy was determined not to exceed 15 cm^3. The clinical target volume exceeded 15 cm^3 in 2 cases, but the lesions in these patients faced the resection cavity or the ventricle, so the volume of the brain parenchyma included in the clinical target volume was <15 cm^3 in both cases. The median clinical target volume of extended field SRS was 13 cm^3 (range, 6-19 cm^3).

Patient Follow-Up and Statistical Analysis

After SRS, follow-up clinical examinations were performed at our hospital or elsewhere by referring physicians. MRI or computed tomography scanning was taken at 1- to 3-month intervals. When a contrast-enhanced lesion continued to grow at follow-up examinations, it was defined as local control failure unless it was histologically confirmed as radiation necrosis. Conversely, if a contrast-enhanced area ceased to expand or decreased in size during the follow-up with or without the use of steroids, the lesion was recognized as radiation necrosis. Statistical analyses were performed using JMP 8 (SAS Institute, Cary, NC). Fisher exact test was performed to evaluate the significance of differences between conventional SRS and extended field SRS regarding the local control rate and the incidence of radiation necrosis, and the correlation between radiation necrosis and the location of treated lesions. The progression-free and overall survival times were calculated using the Kaplan-Meier method. Factors potentially affecting the survival time were evaluated by log-rank test for univariate analysis.

Ethical Issues

The conduct of this study was approved by our institutional review board. All patients provided written informed consent.

RESULTS

Outcomes of Conventional SRS

Characteristics and outcomes of the patients who underwent conventional SRS are summarized in Table 1. Nine patients who underwent SRS targeting gadolinium-enhanced lesions were followed for the median period of 7 months (range, 3-29 months). Among 34 lesions that could be radiographically followed up, 16 lesions (47%) showed <25% increase of the target area or decreased in size in response to SRS until the last follow-up. All patients who died after conventional SRS possessed uncontrolled SRS-treated lesions. The median time to local relapse after SRS was 6 months (range, 1-10 months). The median survival time after the first SRS for recurrences was 10.5 months (range, 3-29 months). The median overall survival time after the diagnosis of glioblastoma was 24 months (range, 14-57 months), and the

6-month overall survival rate was 63%. As for SRS-induced adverse effects, asymptomatic, radiographically confirmed radiation necrosis was observed in 2 lesions in 2 patients (6.5%). Among these 2 lesions, 1 lesion occurred within the clinical target volume of prior radiotherapy and 1 outside ($P = .59$).

Outcomes of Extended Field SRS

Characteristics and outcomes of the patients who underwent extended field SRS are summarized in Table 2. Nine patients who underwent extended field SRS were followed for the median period of 8 months (range, 5-27 months). Thirteen among 14 lesions (93%) showed <25% increase of the target area or decreased in size in response to SRS until the last follow-up. This local control rate was significantly higher than that of conventional SRS ($P = .0035$). The local relapse in the 1 patient (case 2 in Table 2) was histologically confirmed. Whereas the lesions treated by SRS in 8 patients were controlled until the last follow-up, remote recurrences were observed in 5 patients. Two patients (cases 5 and 6 in Table 2) underwent second SRS for those remote lesions. Another patient (case 3 in Table 2) showed a remote recurrence in the brainstem, for which external beam radiotherapy was performed. The median survival time after the first SRS for recurrences was 9 months (range, 6-27 months), and the 6-month overall survival rate was 89%. There was no statistical difference in survival time after SRS between conventional and extended field SRS ($P = .83$). The median overall survival time after the diagnosis of glioblastoma was 21 months (range, 15-51 months), not statistically different from conventional SRS ($P = .71$). Radiation necrosis was observed in 4 lesions in 4 patients (29%), age ranging from 27 to 53 years, and the frequency was not significantly different from conventional SRS ($P = .052$). The irradiated fields for SRS in these 4 patients all involved the irradiated fields of prior radiotherapy, although this was not statistically significant ($P = .25$). All 4 patients required oral administration of prednisolone at doses of 20 to 30 mg (median, 30 mg) for 7 to 25 months (median, 9 months). As for steroid-related toxicities, moon face and central obesity were observed in all 4 patients, and 1 patient experienced urinary tract infection. By the use of oral steroids, radiation necroses became stable and did not cause deterioration of neurological symptoms in any patients. Karnofsky Performance Scale scores of these 4 patients at the time of first SRS were 90%, 70%, 40%, and 70%. Karnofsky Performance Scale score gradually declined in all 4 patients, mainly because of disseminated lesions, and became 70%, 60%, 40%, and 40% at 6 months after first SRS. The 4 patients died of tumor progression at 27, 12, 8, and 14 months after first SRS. Comparison of patient characteristics and treatment outcomes between conventional and extended field SRS is summarized in Table 3.

Table 3. Comparison of Characteristics and Outcomes of the Patients Who Received Conventional SRS and Extended Field SRS

Characteristic	Conventional SRS	Extended Field SRS	*P*
Number of patients	9	9	–
Primary glioblastoma	8	7	1.0
Patient age, median y, range	43, 17-64	53, 27-79	.36
KPS at onset, median, range	90, 80-90	90, 80-90	.62
Time from Dx to 1st SRS, median mo, range	14.5, 1-51	12, 6-39	.66
KPS at 1st SRS, median, range	90, 40-90	70, 40-90	.21
Local control	16/34	13/14	.0035
Radiation necrosis	2/34	4/14	.052
Median OS after Dx, mo	24	21	.71
Median OS after 1st SRS, mo	10.5	9	.83
6-month OS after 1st SRS, %	63	89	.83

Abbreviations: Dx, diagnosis of glioblastoma; KPS, Karnofsky Performance Scale; OS, overall survival; SRS, stereotactic radiosurgery.

Illustrative Cases

A 17-year-old girl (case 7 in Table 1) presented with right hemiparesis. MRI showed a heterogeneously enhanced mass lesion in the left frontal lobe (Fig. 1A). The tumor was subtotally removed and histologically diagnosed as glioblastoma. Boron neutron capture therapy was performed, and temozolomide was administered orally at a dose of 200 mg/m^2 using the 5 of 28-day regimen. Twelve months after the onset, a diffuse recurrence was observed in the left frontal lobe and the corpus callosum, so she received 50-Gy external beam radiotherapy in 25 fractions. At 14 months, a recurrent lesion 7 mm in diameter was noted in the right frontal lobe, and it was treated by conventional SRS targeting the gadolinium-enhanced lesion with a maximum dose of 40 Gy and a margin dose of 20 Gy (Fig. 1B). However, this lesion continued to grow at 1 month (Fig. 1C) and 3 months (Fig. 1D) after the SRS, and the patient died of diffuse dissemination at 3 months after the SRS.

A 53-year-old man (case 1 in Table 2) presented with left hemiparesis. MRI showed a homogeneously enhanced, poorly circumscribed mass lesion in the right frontal lobe (Fig. 2A). The tumor was subtotally removed and histologically diagnosed as glioblastoma. He received 80-Gy external beam radiotherapy in 40 fractions, with

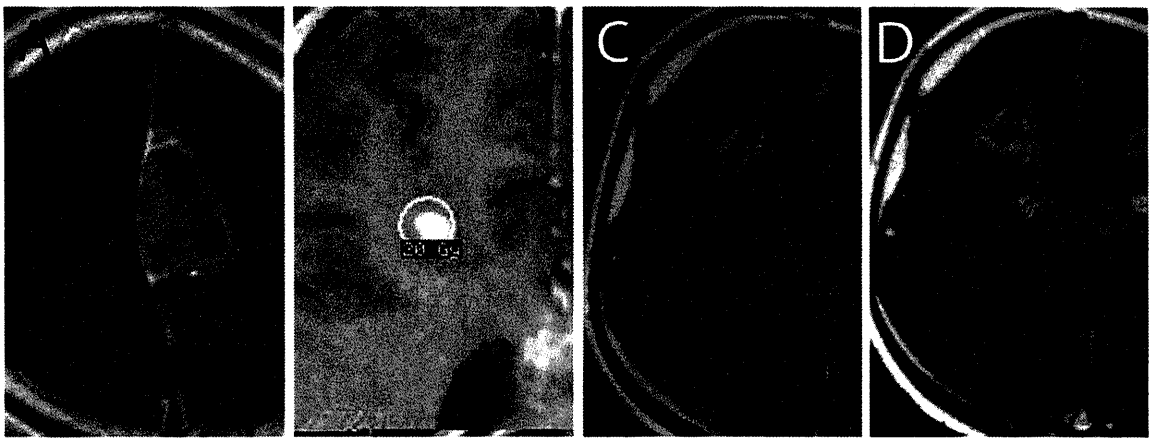

Figure 1. Case 7 in Table 1 is shown: (A) axial gadolinium-enhanced T1-weighted magnetic resonance imaging (MRI) at presentation; (B) dose planning of stereotactic radiosurgery for recurrence; (C, D) MRI taken at 1 (C) and 3 months (D) after stereotactic radiosurgery showing tumor progression.

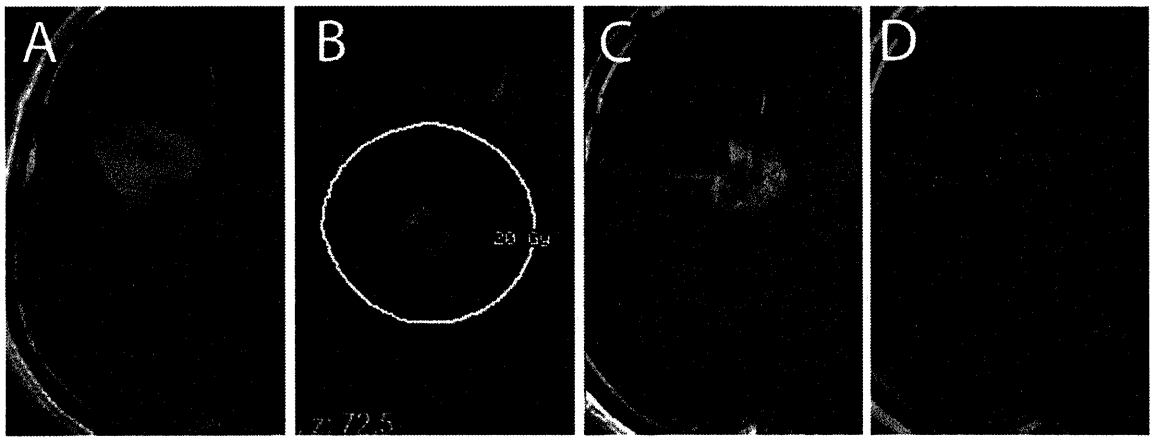

Figure 2. Case 1 in Table 2 is shown: (A) axial gadolinium-enhanced T1-weighted magnetic resonance imaging (MRI) at presentation; (B) dose planning of stereotactic radiosurgery for recurrence; (C) MRI taken at 1 month after stereotactic radiosurgery showing diffuse enhancement around treated lesion; (D) MRI taken at 25 months after stereotactic radiosurgery showing no recurrence.

which temozolomide at a dose of 200 mg/m^2 using the 5 of 28-day regimen was initiated. After the third cycle of temozolomide, eruption and thrombocytopenia were observed, so chemotherapy was switched to nimustine hydrochloride (100 mg/dose), which was administered intravenously once a month thereafter. Although complete remission was maintained until 17 months after the onset, a recurrent lesion 10 mm in diameter was observed near the resection cavity in the right frontal lobe. Extended field SRS was applied to this lesion. The clinical target volume was set as the gadolinium-enhanced lesion plus a 1-cm–wide margin, and 20 Gy was prescribed at the margin of this wide target (Fig. 2B). One month after the SRS, diffuse enhancement around the irradiated area was observed (Fig. 2C). As radiation necrosis was suspected, oral prednisolone at a dose of 30 mg daily was initiated, and the area of enhancement ceased to expand thereafter. At 25-month follow-up after the SRS, the treated lesion had been locally controlled, and no new recurrence was noted (Fig. 2D).

A 27-year-old man (case 2 in Table 2) presented with right hemiparesis. MRI revealed a homogeneously enhanced mass in the right frontal lobe (Fig. 3A). Stereotactic biopsy was performed, and the diagnosis of glioblastoma was obtained. He received 60-Gy external beam radiotherapy followed by adjuvant temozolomide at a dose of 200 mg/m^2 using the 5 of 28-day regimen. Complete remission was achieved and maintained until 39 months after the onset, when a recurrent lesion (maximal diameter, 15 mm) was noted in the right frontal lobe

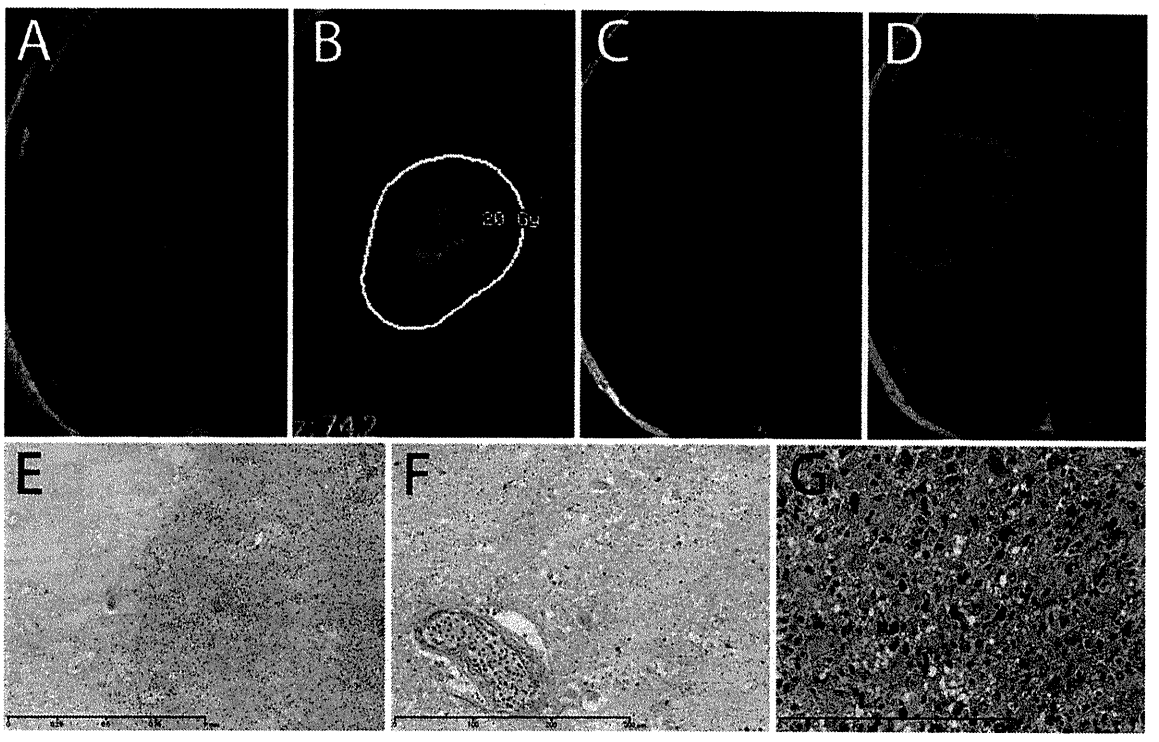

Figure 3. Case 2 in Table 2 is shown. (A) Axial gadolinium-enhanced T1-weighted magnetic resonance imaging (MRI) at presentation is shown. (B) Dose planning of stereotactic radiosurgery for recurrence. (C) MRI taken at 5 month after stereotactic radiosurgery revealed progression of enhancing lesion around the treated area. (D) MRI taken at 12 months after stereotactic surgery revealed continued tumor growth. (E-G) Hematoxylin and eosin staining of a surgical specimen at recurrence (E) revealed focuses of radiation necrosis (F) surrounded by an area of tumor with high cellularity (G).

beneath the wall of the right lateral ventricle. This recurred lesion was treated by extended field SRS targeting the gadolinium-enhanced lesion plus a 1-cm–wide margin. Prescribed margin dose was 20 Gy (Fig. 3B). Heterogeneous enhancement appeared at the irradiated site 1 month after the SRS and continued to grow despite the use of oral prednisolone. Frontal lobectomy was performed 5 months after the SRS to decrease the tumor mass that caused deterioration of the consciousness level (Fig. 3C). Recurrence of glioblastoma was confirmed by a histological examination, and the tumor continued to grow diffusely after the surgery. The patient died of tumor progression 12 months after the SRS for recurrence (Fig. 3D). Histologically, the surgical specimens at recurrence (Fig. 3E) consisted of focal areas of radiation necrosis (Fig. 3F) surrounded by areas of viable tumors with high cellularity consistent with glioblastoma (Fig. 3G).

DISCUSSION

Our results showed that extended field SRS potentially provided improved local control of isolated recurrence of glioblastoma without causing uncontrollable symptomatic radiation necrosis. In several studies analyzing patients treated with radiation and temozolomide, 72% to 92% of recurrence was revealed as local relapse,[25,26] the most frequent pattern of glioblastoma recurrence.[6] Local control is also important for recurrent lesions, but treatment with SRS led to local progression in 65% to 90%,[14,27-29] which was in line with our result with conventional SRS targeting only the gadolinium-enhanced area. The logical assumption regarding the reason for this lack of efficacy is that SRS, owing to its characteristic feature of steep dose falloff, is unable to kill tumor cells infiltrating the tissue outside the irradiated field.[20,27] When we extended the irradiation field with the intent to include as many tumor cells invasive to the surrounding tissue as possible, we achieved a high local control rate of 93%. This result showed that extended field SRS was highly effective in controlling recurrent glioblastoma for selected patients found with small lesions. One limitation of this treatment is that it is not applicable to lesions larger than approximately 20 mm in diameter. Adding a sufficient margin to a large lesion results in a large prescribed isodose volume, and may cause uncontrollable radiation-

induced adverse events. A close radiological follow-up after the initial treatment is necessary to detect such small recurrent lesions for this treatment to be suitable for an extended field SRS application. Stereotactic fractionated radiotherapy may be 1 treatment option for larger recurrent lesions. By using 11-C-methionine positron emission tomography for targeting, stereotactic fractionated radiotherapy was reported to have achieved the median survival time of 9 months.[30] Although the incidence of radiation necrosis after SRS was not significantly different between conventional and extended field SRS, all patients who developed radiation necrosis after extended field SRS required steroid administration. This risk of eventual necessity of steroid administration may be another limitation of this approach.

Whereas extended field SRS achieved a high local tumor control rate, it did not show a significant survival benefit compared with conventional SRS in our study. All patients treated with extended field SRS received external beam radiation therapy and temozolomide before SRS. The majority of patients treated with extended field SRS died of remote recurrences within the brain. Because the rates of new recurrences in patients treated with temozolomide and radiation are quite high to begin with, 25% at 1 year and 66% at 2 years,[26] the role of extended field SRS for the occurrence of remote recurrences is unclear. Obviously, radiation therapy, including SRS, and temozolomide are not sufficient to control the disease. New approaches are underway, including monoclonal antibodies that target specific molecules, for example, bevacizumab,[31,32] and oncolytic viruses that replicate selectively in tumor cells.[33]

In conclusion, extended field SRS was well tolerated and superior to conventional SRS in the local control of small recurrent lesions of glioblastoma, although a further device to suppress remote recurrences may be necessary to improve survival.

FUNDING SOURCES

No specific funding was disclosed.

CONFLICT OF INTEREST DISCLOSURES

The authors made no disclosures.

REFERENCES

1. Louis DN, Ohgaki H, Wiestler OD, Cavenee WK. World Health Organization Histological Classification of Tumours of the Central Nervous System. 4th ed. Lyon, France: International Agency for Research on Cancer; 2007.
2. Stupp R, Mason WP, van den Bent MJ, et al. Radiotherapy plus concomitant and adjuvant temozolomide for glioblastoma. *N Engl J Med.* 2005;352:987-996.
3. Dirks P, Bernstein M, Muller PJ, Tucker WS. The value of reoperation for recurrent glioblastoma. *Can J Surg.* 1993;36:271-275.
4. Larson DA, Suplica JM, Chang SM, et al. Permanent iodine 125 brachytherapy in patients with progressive or recurrent glioblastoma multiforme. *Neuro Oncol.* 2004;6:119-126.
5. Wong ET, Hess KR, Gleason MJ, et al. Outcomes and prognostic factors in recurrent glioma patients enrolled onto phase II clinical trials. *J Clin Oncol.* 1999;17:2572-2578.
6. Chang SM, Parney IF, Huang W, et al. Patterns of care for adults with newly diagnosed malignant glioma. *JAMA.* 2005;293:557-564.
7. Hau P, Baumgart U, Pfeifer K, et al. Salvage therapy in patients with glioblastoma: is there any benefit? *Cancer.* 2003;98:2678-2686.
8. Kano H, Niranjan A, Kondziolka D, Flickinger JC, Lunsford LD. Outcome predictors for intracranial ependymoma radiosurgery. *Neurosurgery.* 2009;64:279-287.
9. Kinoshita M, Izumoto S, Kagawa N, Hashimoto N, Maruno M, Yoshimine T. Long-term control of recurrent anaplastic ependymoma with extracranial metastasis: importance of multiple surgery and stereotactic radiosurgery procedures—case report. *Neurol Med Chir (Tokyo).* 2004;44:669-673.
10. Endo H, Kumabe T, Jokura H, Shirane R, Tominaga T. Stereotactic radiosurgery for nodular dissemination of anaplastic ependymoma. *Acta Neurochir (Wien).* 2004;146:291-298.
11. Kano H, Kondziolka D, Niranjan A, Flickinger JC, Lunsford LD. Stereotactic radiosurgery for pilocytic astrocytomas part 1: outcomes in adult patients. *J Neurooncol.* 2009;95:211-218.
12. Koga T, Morita A, Maruyama K, et al. Long-term control of disseminated pleomorphic xanthoastrocytoma with anaplastic features by means of stereotactic irradiation. *Neuro Oncol.* 2009;11:446-451.
13. Larson DA, Gutin PH, McDermott M, et al. Gamma knife for glioma: selection factors and survival. *Int J Radiat Oncol Biol Phys.* 1996;36:1045-1053.
14. Souhami L, Seiferheld W, Brachman D, et al. Randomized comparison of stereotactic radiosurgery followed by conventional radiotherapy with carmustine to conventional radiotherapy with carmustine for patients with glioblastoma multiforme: report of Radiation Therapy Oncology Group 93-05 protocol. *Int J Radiat Oncol Biol Phys.* 2004;60:853-860.
15. Kondziolka D, Flickinger JC, Bissonette DJ, Bozik M, Lunsford LD. Survival benefit of stereotactic radiosurgery for patients with malignant glial neoplasms. *Neurosurgery.* 1997;41:776-783.
16. Chamberlain MC, Barba D, Kormanik P, Shea WM. Stereotactic radiosurgery for recurrent gliomas. *Cancer.* 1994;74:1342-1347.
17. Kong DS, Lee JI, Park K, Kim JH, Lim DH, Nam DH. Efficacy of stereotactic radiosurgery as a salvage treatment for recurrent malignant gliomas. *Cancer.* 2008;112:2046-2051.
18. Combs SE, Widmer V, Thilmann C, Hof H, Debus J, Schulz-Ertner D. Stereotactic radiosurgery (SRS): treatment option for recurrent glioblastoma multiforme (GBM). *Cancer.* 2005;104:2168-2173.
19. Mehta MP, Masciopinto J, Rozental J, et al. Stereotactic radiosurgery for glioblastoma multiforme: report of a prospective study evaluating prognostic factors and analyzing long-term survival advantage. *Int J Radiat Oncol Biol Phys.* 1994;30:541-549.
20. Masciopinto JE, Levin AB, Mehta MP, Rhode BS. Stereotactic radiosurgery for glioblastoma: a final report of 31 patients. *J Neurosurg.* 1995;82:530-535.
21. Wallner KE, Galicich JH, Krol G, Arbit E, Malkin MG. Patterns of failure following treatment for glioblastoma multiforme and anaplastic astrocytoma. *Int J Radiat Oncol Biol Phys.* 1989;16:1405-1409.
22. Hochberg FH, Pruitt A. Assumptions in the radiotherapy of glioblastoma. *Neurology.* 1980;30:907-911.
23. Massager N, Maris C, Nissim O, Devriendt D, Salmon I, Levivier M. Experimental analysis of radiation dose distribution in radiosurgery. II. Dose fall-off outside the target volume. *Stereotact Funct Neurosurg.* 2009;87:137-142.
24. Schiffer D, Cavalla P, Dutto A, Borsotti L. Cell proliferation and invasion in malignant gliomas. *Anticancer Res.* 1997;17:61-69.
25. Brandes AA, Tosoni A, Franceschi E, et al. Recurrence pattern after temozolomide concomitant with and adjuvant to radiotherapy in

newly diagnosed patients with glioblastoma: correlation with MGMT promoter methylation status. *J Clin Oncol.* 2009;27:1275-1279.
26. Milano MT, Okunieff P, Donatello RS, et al. Patterns and timing of recurrence after temozolomide-based chemoradiation for glioblastoma. *Int J Radiat Oncol Biol Phys.* 2010;78:1147-1155.
27. Pouratian N, Crowley RW, Sherman JH, Jagannathan J, Sheehan JP. Gamma Knife radiosurgery after radiation therapy as an adjunctive treatment for glioblastoma. *J Neurooncol.* 2009;94:409-418.
28. Shrieve DC, Alexander E III, Black PM, et al. Treatment of patients with primary glioblastoma multiforme with standard postoperative radiotherapy and radiosurgical boost: prognostic factors and long-term outcome. *J Neurosurg.* 1999;90:72-77.
29. Sarkaria JN, Mehta MP, Loeffler JS, et al. Radiosurgery in the initial management of malignant gliomas: survival comparison with the RTOG recursive partitioning analysis. Radiation Therapy Oncology Group. *Int J Radiat Oncol Biol Phys.* 1995;32:931-941.
30. Grosu AL, Weber WA, Franz M, et al. Reirradiation of recurrent high-grade gliomas using amino acid PET (SPECT)/CT/MRI image fusion to determine gross tumor volume for stereotactic fractionated radiotherapy. *Int J Radiat Oncol Biol Phys.* 2005;63:511-519.
31. Gutin PH, Iwamoto FM, Beal K, et al. Safety and efficacy of bevacizumab with hypofractionated stereotactic irradiation for recurrent malignant gliomas. *Int J Radiat Oncol Biol Phys.* 2009;75:156-163.
32. Vordermark D, Kolbl O, Ruprecht K, Vince GH, Bratengeier K, Flentje M. Hypofractionated stereotactic re-irradiation: treatment option in recurrent malignant glioma. *BMC Cancer.* 2005;5:55.
33. Todo T. Oncolytic virus therapy using genetically engineered herpes simplex viruses. *Front Biosci.* 2008;13:2060-2064.

JOURNAL OF APPLIED CLINICAL MEDICAL PHYSICS, VOLUME 13, NUMBER 1, 2012

Investigation of the feasibility of a simple method for verifying the motion of a binary multileaf collimator synchronized with the rotation of the gantry for helical tomotherapy

Masatoshi Hashimoto,[1,2a] Masahiro Uematsu,[2] Makiko Ito,[2] Yukihiro Hama,[2] Takayuki Inomata,[3] Masahiro Fujii,[4] Teiji Nishio,[5] Naoki Nakamura,[6] Keiichi Nakagawa[1]

Division of Radiology and Biomedical Engineering,[1] Graduate School of Medicine, The University of Tokyo, Bunkyo-ku, Tokyo, Japan; Department of Radiology,[2] Tokyo Edogawa Cancer Center, Edogawa Hospital, Edogawa-ku, Tokyo, Japan; Department of Radiology,[3] International University of Health and Welfare Atami Hospital, Atami-shi, Shizuoka, Japan; Department of Radiology,[4] Shinshu University Hospital, Matsumoto-shi, Nagano, Japan; Particle Therapy Division,[5] Research Center for Innovation Oncology, National Cancer Center Hospital East, Kashiwa-shi, Chiba, Japan; Department of Radiation Oncology,[6] St. Luke's International Hospital, Chuo-ku, Tokyo, Japan
m_hashimoto@movie.ocn.ne.jp

Received 9 February, 2011; accepted 26 July, 2011

In this paper, we suggest a new method for verifying the motion of a binary multileaf collimator (MLC) in helical tomotherapy. For this we used a combination of a cylindrical scintillator and a general-purpose camcorder. The camcorder records the light from the scintillator following photon irradiation, which we use to track the motion of the binary MLC. The purpose of this study is to demonstrate the feasibility of this method as a binary MLC quality assurance (QA) tool. First, the verification was performed using a simple binary MLC pattern with a constant leaf open time; secondly, verification using the binary MLC pattern used in a clinical setting was also performed. Sinograms of simple binary MLC patterns, in which leaves that were open were detected as "open" from the measured light, define the sensitivity which, in this case, was 1.000. On the other hand, the specificity, which gives the fraction of closed leaves detected as "closed", was 0.919. The leaf open error identified by our method was -1.3 ± 7.5%. The 68.6% of observed leaves were performed within ± 3% relative error. The leaf open error was expressed by the relative errors calculated on the sinogram. In the clinical binary MLC pattern, the sensitivity and specificity were 0.994 and 0.997, respectively. The measurement could be performed with -3.4 ± 8.0% leaf open error. The 77.5% of observed leaves were performed within ± 3% relative error. With this method, we can easily verify the motion of the binary MLC, and the measurement unit developed was found to be an effective QA tool.

PACS numbers: 87.56.Fc, 87.56.nk

Key words: helical tomotherapy, verification, multileaf collimator, plastic scintillator

I. INTRODUCTION

The demand for the use of high-technology in radiation therapy is rapidly increasing. In order to concentrate the radiation dose in the tumor, the use of intensity-modulated radiation therapy (IMRT)[1-4] has become more widespread. With the technological advances made in IMRT, it has

[a] Corresponding author: Masatoshi Hashimoto, Department of Radiology, Tokyo Edogawa Cancer Center, Edogawa Hospital, 2-14-18 Higashi Koiwa, Edogawa-ku, Tokyo 133-0052, Japan; phone: +81-3-3673-1221; fax:+81-3673-1229; email: m_hashimoto@movie.ocn.ne.jp

become possible to deliver more complex radiation fields to the target; however, simultaneous verification of the appropriateness of the radiation field also needs to be done. Verification using ion chambers and film is common, and these are well known quality assurance (QA) tools,[5] but are basically used for measuring the cumulative dose or radiation field.

New IMRT methods using dynamic multileaf collimators (MLC)[6-9] and helical tomotherapy (TomoTherapy Inc., Hi·Art, Madison, WI)[10-12] have been developed and these are now used worldwide. In these methods, the MLC is moved during irradiation and, therefore, its motion must be very precisely controlled. To accurately measure the MLC motion, dynamic observations of it need to be made; however, commercial products[13-16] for this are generally too expensive. Thus, it has been very difficult to perform such measurements in most treatment facilities or hospitals. Helical tomotherapy, composed of a small 6 MV linear accelerator rotating on a slip ring together with a binary MLC, enables us to deliver a complex dose distribution. The motion pattern of the binary MLC needs to be synchronized with the rotation of the gantry. However, a tool for measuring such motion has not been readily available.

To address this shortcoming, we used a cylindrical plastic scintillator for measuring dose. The classical way of taking measurements with a scintillator is to use a photomultiplier tube (PMT) attached to the scintillator in a light-proof box.[17] Furthermore, Beddar et al.[18,19] reported that it is possible to measure high-energy photons and electrons with the detector made of the PMT attached with optical fibers. More recently, built-in charge-coupled device (CCD) cameras and optical fibers have been used.[20,21] Special skills and knowledge are required to build these units. We have developed a similar method that is much simpler to implement. In our method, we use a general-purpose camcorder instead of a CCD unit. The camcorder is used to record the light image from the scintillator. This method has previously been used for measuring the range of proton and carbon particles and also for QA in brachytherapy and diagnostic computed tomography.[22-30] We investigated combining these simple devices to measure a complex IMRT field, and also examined the feasibility of using this as a tomotherapy QA technique.

II. MATERIALS AND METHODS

A. System setup for measurement

The scintillator used was a cylindrical plastic scintillator (20 cm in diameter by 10 cm in length, Rexon Components, Inc., RP-400, Beachwood, OH), composed of H and C only, with a density of 1.302 g/cm^3. The benefits of plastic scintillators are that they have quicker rise times and shorter decay times than inorganic scintillators. The refractive index was 1.58, the rise time, 0.9 nsec, and the decay time, 2.4 nsec.

Figure 1 shows the measurement setup. The plastic scintillator was placed in a helical tomotherapy gantry so that the center of the scintillator was aligned to the isocenter of the gantry. Megavoltage computed tomography (MVCT) was used to precisely position the scintillator. A camcorder (Sony corp., HDR-HC7, Tokyo) was set at a distance of 100 cm from the isocenter. The camcorder was connected to a personal computer through an IEEE cable, and the scintillation light was recorded as 8-bit gray scale, 640 × 480 resolution images at 29.97 frames per second (fps). It was previously found that recording an 8-bit gray scale image would be sufficient for this QA feasibility study.[23-25] Other settings (e.g., zoom, focus, and sensitivity) were left unchanged. During recording, the room was made as dark as possible. At 29.97 fps, an image can be taken every 33 msec. Under these conditions, our system was able to detect the light and to verify the dynamic motion of the binary MLC and the motion of the rotating gantry. The detected light was converted into image datasets for each and every frame and used for analysis.

Due to the geometrical limitations of the 20 cm diameter scintillator, it was possible to monitor the radiation field only from leaf number 18 to leaf number 47. Figure 2(a) shows the image from the scintillator of a 6 MV X-ray collimated radiation field of 2.5 cm × 10 cm.

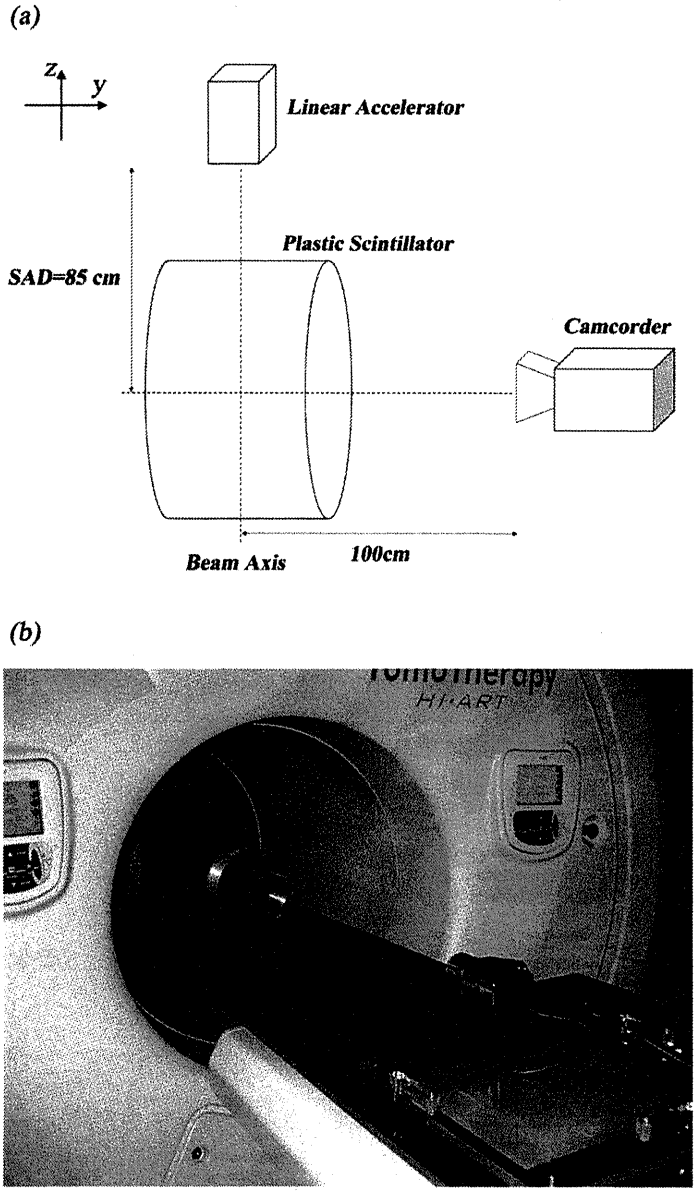

FIG. 1. Schematic (a) and photograph (b) of the measurement setup. The center of the plastic scintillator is irradiated with X-rays. The coordinate system follows the Left-hand coordinate system. SAD in this figure stands for the source–axis distance.

Figure 2(b) shows the image with the even number collimators opened. For measurement of the light, regions of interest (ROI) of 5 × 5 pixels (1 pixel = 0.468 × 0.468 mm^2) have been placed on each area corresponding to each leaf number in the image. The average pixel value in the jth ROI of the ith frame is defined as $q_{raw\,ji}$, and the quantity of the light detected in each frame was calculated by subtracting the background value, BG, from $q_{raw\,ji}$ in each ROI:

$$q_{ji}\ (\text{pixel value}) = q_{raw\,ji} - BG \tag{1}$$

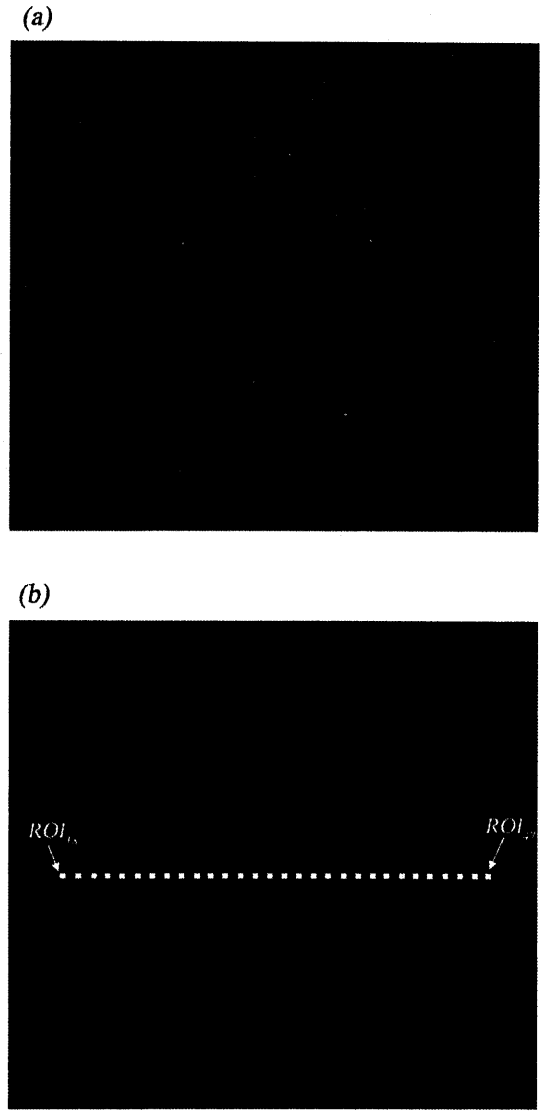

FIG. 2. Scintillation light emitted from a 2.5 × 10 cm^2 field (a), and scintillation light emitted in the case in which the even number leaf positions are open (b). The white boxes are ROIs used to measure the detected light. The ROIs are set at the center of the leaves.

Accumulating q_{ji} over the sampling frames, we get

$$Q_j \text{ (pixel value)} = \sum_i q_{ji} \tag{2}$$

We use Q for the amount of light measured over all frames and ROI positions. BG is obtained from the average $q_{raw\,ji}$ measured in nonexposure (e.g., $q_{raw\,ji}$ averaged over 9000 frames was 0.36). This was used as the value of BG in this study.

Under these measurement settings, photons scattered from the collimator rarely, but sometimes, interact with the camcorder and give rise to noise. Such noise is called transient noise, and it is possible to reduce this noise by surrounding the camcorder with radiation shielding material. It is also possible to correct for noise in the images by applying a spatial filtering algorithm (e.g., a median filter). However, it turns out that the filtering correction alters each

pixel value.[31] In our preclinical tests on the scintillation light detection system, we exposed the scintillator to a 2.5 cm × 10 cm field of 6 MV X-rays and recorded the light for 300 sec (equivalent to 9000 frames). We observed noise 18 times in the 9000 images, which indicates the probability of transient noise to be 0.2% per frame. This is lower than the noise in similar systems using CCDs. Therefore, for these measurements, neither image filtering nor radiation shielding for noise correction was done.

B. Characteristics of light detection

In order to verify implementation of the unit as a QA tool, we conducted some basic measurements which are performed in the QA procedure for helical tomotherapy. For the first step, these were done under static field conditions with the gantry angle at 0° and exposure to 6 MV X-rays at a dose rate of 839 cGy/min.

B.1 Relationship between the scintillation light and the collimator open time

It is important to understand the characteristics of the light detected from this system in order to be able to use it to predict the time for which the collimator is open (defined as "leaf open time"). First, we investigated the relationship between the light and the leaf open time from the measurements. The field size was 2.5 cm × 10 cm (opening leaf numbers 25–40). We changed the leaf open time from 29.41 msec to 294.12 msec and made measurements in each case. For these measurements, the value of Q at the isocenter, Q_{center}, is defined as a reference point. Since the isocenter for tomotherapy is located between leaf numbers 32 and 33, this was calculated from the following:

$$Q_{center} \text{ (pixel value)} = (Q_{32}+Q_{33}) / 2 \tag{3}$$

B.2 Lateral profile in the scintillator

The lateral profile in the plastic scintillator is different from the one given by a conventional measurement (e.g., film or 2D profile detector and 3D water measurement), due to the cylindrical shape of the plastic scintillator. Thus, a reference profile for the cylindrical shape is required. This was done by opening a single leaf and exposing the detector to 6 MV X-rays for 294.12 msec. This process was repeated for all the leaves from 18 to 47, during which time the camcorder was recording the light continuously. Subsequently, we obtained measurements for each Q_j (j = 18 to 47).

B.3 Field size dependency of the detected light

The profile measurement was also performed for several field sizes, where the effective field size ranged from 0.625 cm to 17.5 cm. The exposure time was 294.12 msec. We observed each Q_j value, and also looked at the output factor on the central axis.

B.4 Exposure time and the detected light

The field size was 10 cm with the 25th–40th leaves opened. The exposure time was 300 sec. The $q_{center\ i}$ value for each frame was observed frame by frame. We also performed measurements with an ion chamber (Standard Imaging, Inc., A12, Middleton, WI) and a Tomotherapy Electrometer Measurement System (TomoTherapy Inc., Madison, WI). The chamber was placed at the center at a depth of 10 cm in a solid phantom in the same field. The sample time for the ion chamber was 250 msec.

C. Gantry rotation speed measurement (rotational stability)

The benefit of measurements using the cylindrically shaped detector is the capability of performing dynamic measurements of the rotating gantry in a helical tomotherapy unit. In this measurement, the scintillation light signals are recorded during the gantry rotation, and by

observing these we verified if the gantry rotation speed varies at each gantry angle. An X-ray field along the central axis was established by opening either leaf 32 or 33, and the gantry speed was set to rotate at from 15 to 60 sec per revolution. The narrow beam profiles were recorded frame by frame, from which we observed the position of the beam profile whose side passed through the isocenter.

D. Binary MLC QA using the cylindrical scintillator

Helical tomotherapy requires a sinogram file to control the motion of the binary MLC. The file consists of each leaf number expressed in the horizontal axis and its corresponding projection number in the vertical axis. In the sinogram, the leaf open times of each leaf number for each projection are given by a number between 0.0 and 1.0. Here 0.0 means that the leaf is closed. For helical tomotherapy, 51 projections can be delivered in one gantry rotation. Suppose one complete rotation of the gantry takes 15 seconds, then one projection needs 294.12 msec (equivalent to 15 secs/51). Therefore, the leaf open time is expressed by the fraction of 294.12 msec. For example, 0.5 expressed in the sinogram means that the leaf open time is 147.06 ms, which is half of 294.12 msec. In a clinical situation, the minimum leaf open time is about 20 msec.

The feasibility of using the scintillator unit as a QA tool was investigated. We attempted to perform the binary MLC QA using the measured q_{ji}. The sinogram was reconstructed from the measured q_{ji} and was compared with the original sinogram dataset. q_{ji} is the detected light per frame. The sinogram represents the leaf open time for each projection. In order to reconstruct the sinogram, q_{ji} needs to be summed for each projection. The summed q_{ji} is converted into the leaf open time. For the conversion, we used the relationship between the detected light and the leaf open time, which is made based upon the measurement at the center of the plastic scintillator (see Section B.1 above). In this relationship, q_j needs to be normalized because if each q_j (acquired under the condition that each leaf is open for a certain time) is different from each other, it leads to error. There is another cause of error in that the detected light changes due to exposure time. This also needs to be handled. In this study, two correction factors are applied for each leaf position: one is for correcting the difference in the detected light, k_{1j}, and the other is for correcting time variances, k_{2i}. The corrected value of the detected light is defined as q_{cji} as follows:

$$q_{cji} \text{ (pixel value)} = q_{ji} \cdot k_{1j} \cdot k_{2i} \tag{4}$$

Here, k_{1j} and k_{2i} are the lateral profile of the jth ROI and the exposure time correction for the ith frame mentioned in previous sections. In the scintillator and camcorder unit, there may be some issues with respect to the detection of light scattered in the medium and Cherenkov radiation. These phenomena can cause spurious signals in nonexposed ROIs and, in order to deal with these, we set a threshold (Th) to the ROI signal for the scintillation light measurement. Ideally, the threshold values for each ROI bin are derived from the field size effect (output factor in each ROI area) discussed in Section B.3 above. For the purpose of a much simpler verification method, we attempted to determine a general threshold value from the descriptive field size effect measured at center of the field. The threshold value was determined by a receiver operating characteristic (ROC) curve. The q_{cji} is finally normalized in order to agree with the real exposure time in the original sinogram using the relationship between the exposure time and q measured in section Section B.1 above.

The measurement was performed with the gantry rotating. The gantry was rotated at a constant velocity of 15 sec per revolution. Dose distributions corresponding to the binary leaf patterns show up on the scintillator surface, and the camcorder records these at each gantry angle.

Since the ROIs put on the image in Fig. 2 are fixed at each position and these do not rotate with the gantry rotation, it is not a real-time measurement. Following the light acquisition for all gantry angles, each of the images acquired are rotated back to 0°, by which we measured

the q_{ji} at each gantry angle. The actual appropriate gantry angles to rotate the images back were given from the result of Section C above. In this way, it is possible to conduct a real-time binary MLC QA with the rotating gantry during treatment. This is the benefit of this measurement. In the procedure, two sets of sinograms were used. One was a very simple sinogram in which all of the binary MLCs were open for 294.12 msec and this was repeated for 133 projections (simple binary MLC pattern). Another set was the clinical case of a prostate treatment MLC pattern, with 643 projection data and a modulation factor of 1.649 (clinical binary MLC pattern). The modulation factor is defined by maximum leaf open time divided by the average leaf open time. When the modulation factor increases, the leaf open time becomes shorter on the sinogram. In the measurements, the treatment couch was not moved and the number of projections was fixed at 51. The sinogram was analyzed based on the Th value. When q_{cji} was greater than Th, the jth leaf was identified as being open. When q_{cji} was less than Th, the jth leaf was considered to be closed. The suitability of the Th value was also evaluated by considering the sensitivity and specificity for some sets of Th values. The leaf open time obtained from this method was compared with the one for the original sinogram data.

III. RESULTS

A. Characteristics of light detection

A.1 Relationship between scintillation light and collimator open time

The relationship between the detected light Q at the central beam axis, between the 32nd and 33rd leaf positions, is shown in Fig. 3. Good linearity can be seen for leaf open times from 29.41 msec to 294.12 msec. This has already been reported,[25,29] and we were able to obtain a similar result. The relationship shows that by changing the leaf open time, we can control the exposure to the scintillator and, conversely, that it is possible to predict the leaf open time from the detected light Q.

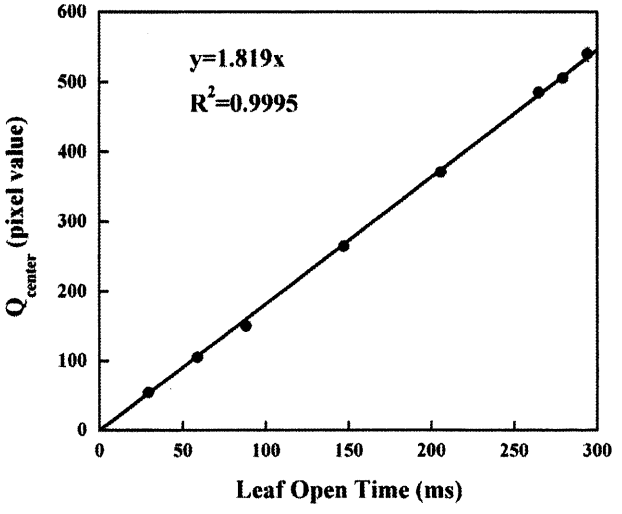

FIG. 3. Relationship between the leaf open time and detected light. Q_{center}, on the vertical axis, is calculated from Eq. (3).

A.2 Lateral profile in the scintillator

The result of the lateral profile using the scintillator unit is shown in Fig. 4. There is a slight slope in the profile from the center of the beam line towards the off-axis direction. The main reasons for this are that there is no flattening filter in the linear accelerator used for helical tomotherapy, and the depth doses at each ROI position are different in the cylindrical scintillator. Each value, q_j, is normalized to the 32nd detected light value, q_{32}, which is at the center of the field. The inverse value of the relative value in the profile is used for k_{1j}.

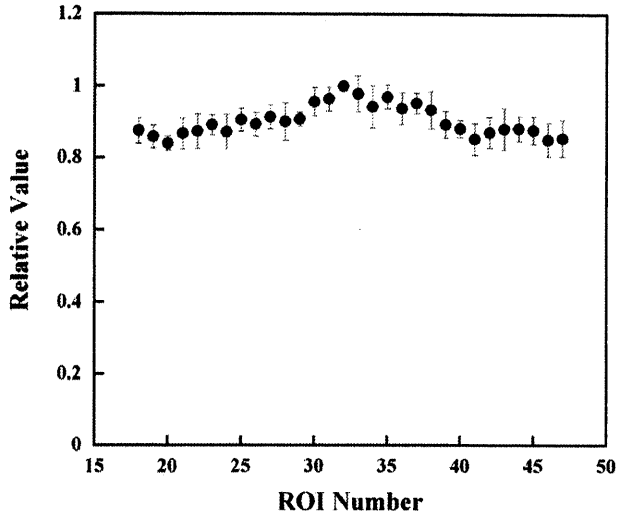

FIG. 4. Measured light on each ROI in the case in which each leaf was open individually. These are normalized by the light on the 32nd ROI.

A.3 Field size dependency of the detected light

The relationship between the field size and the beam profile is shown in Fig. 5(a). The Q_j in each ROI increases as the field size is widened. This is caused by scattered photons, light scattering[25,29] and Cherenkov radiation[26,32,33] in the scintillator. Figure 5(b) shows the output factors in terms of Q_j at the center and at the field edge for each field size in Fig. 5(a). The center is at the 32nd leaf position when opening one leaf, and between leaves 32 and 33 when opening two or more leaves. The Q at the field edge is defined, when the leaves from j to j+n are open, as the average value of Q_{j-1} and Q_{j+n+1}. For example, when just the 32nd leaf is open, the field edge is the average of Q_{31} and Q_{33}, and when the 32nd–33rd leaves are open, the field edge is the average of Q_{31} and Q_{34}. The detected light per frame at center increases from 29.1 up to 65.1 pixel value. In the field edge, the detected light per frame increased from 5.6 to 33.7 pixel value. The light detected at the center when just one leaf was open is lower than the light detected at the field edge when 24 leaves were open (Fig. 5(b)). This means that, in the case of the wider field shown in Fig. 5(a), even if a few leaves are not open at the side, the unopened leaves might possibly be recognized as being "open". This might be the cause of errors in this measurement.

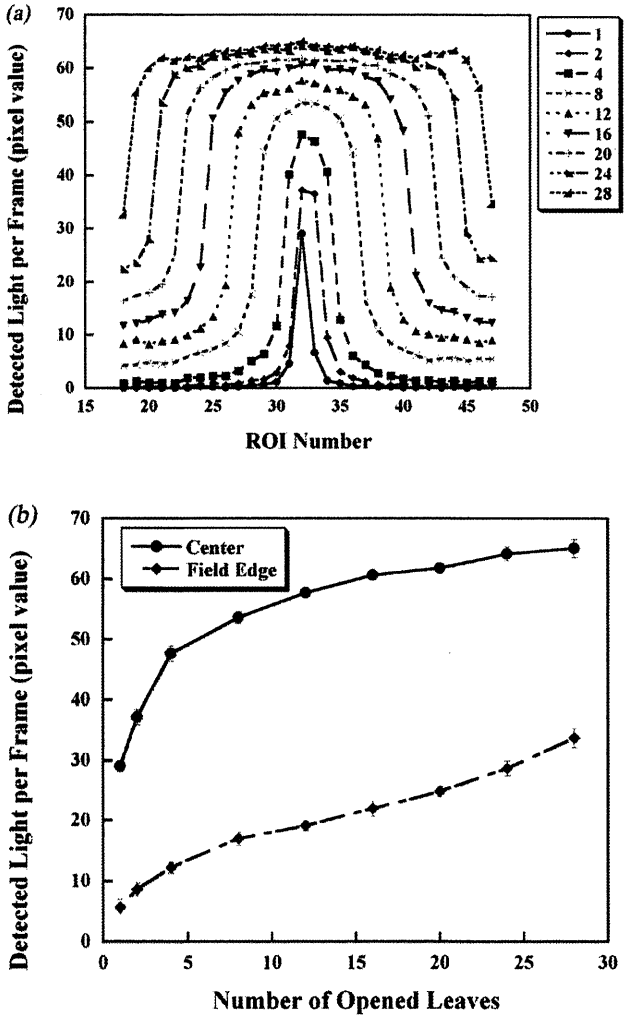

FIG. 5. Field dependency of the measured light: the light measured at each ROI and its corresponding leaf position (a); the number of open leaves and the output factor at the central axis and in the field edge region (b). The vertical axis is the detected light per frame.

A.4 Exposure time and the detected light

The relationship between irradiation time and the scintillation light detected (relative value) on the camcorder is shown in Fig. 6. The detected light is slightly greater than 1 for short irradiation times, and then gradually decreases. Since this trend is also seen in the ion chamber measurements, it is thought that the slight variation was due to a variation in the beam output and not to the scintillator. However, since the variation in the beam output affects the results, a correction factor k_{2i} for the beam output based on this curve was applied.

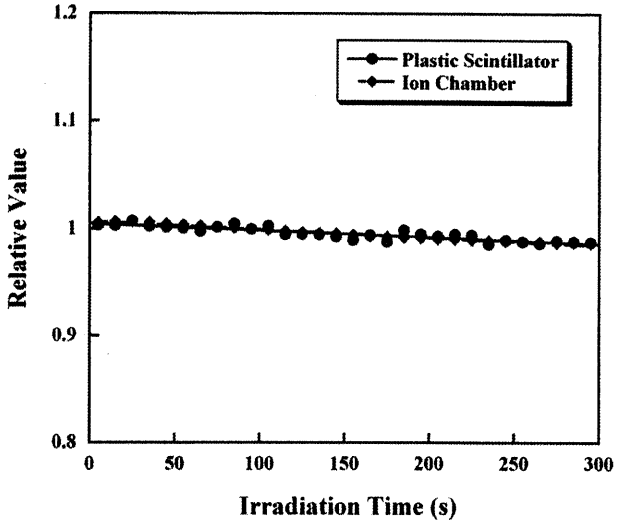

FIG. 6. Stability of the data measured with an ion chamber and the plastic scintillator. The measured data from the scintillator are based on $q_{center\,i}$. The data from the ion chamber are from measurements made at a depth of 10 cm. Each plot is averaged over a time of 10 sec and normalized by the value at 100 sec. The readings of both the plastic scintillator and ion chamber decreased with exposure time.